TECHNICAL REVIEW

Primary Calibration using Laser Interferometry
Infrasound Calibration of Microphones
High-temperature IEPE Accelerometer

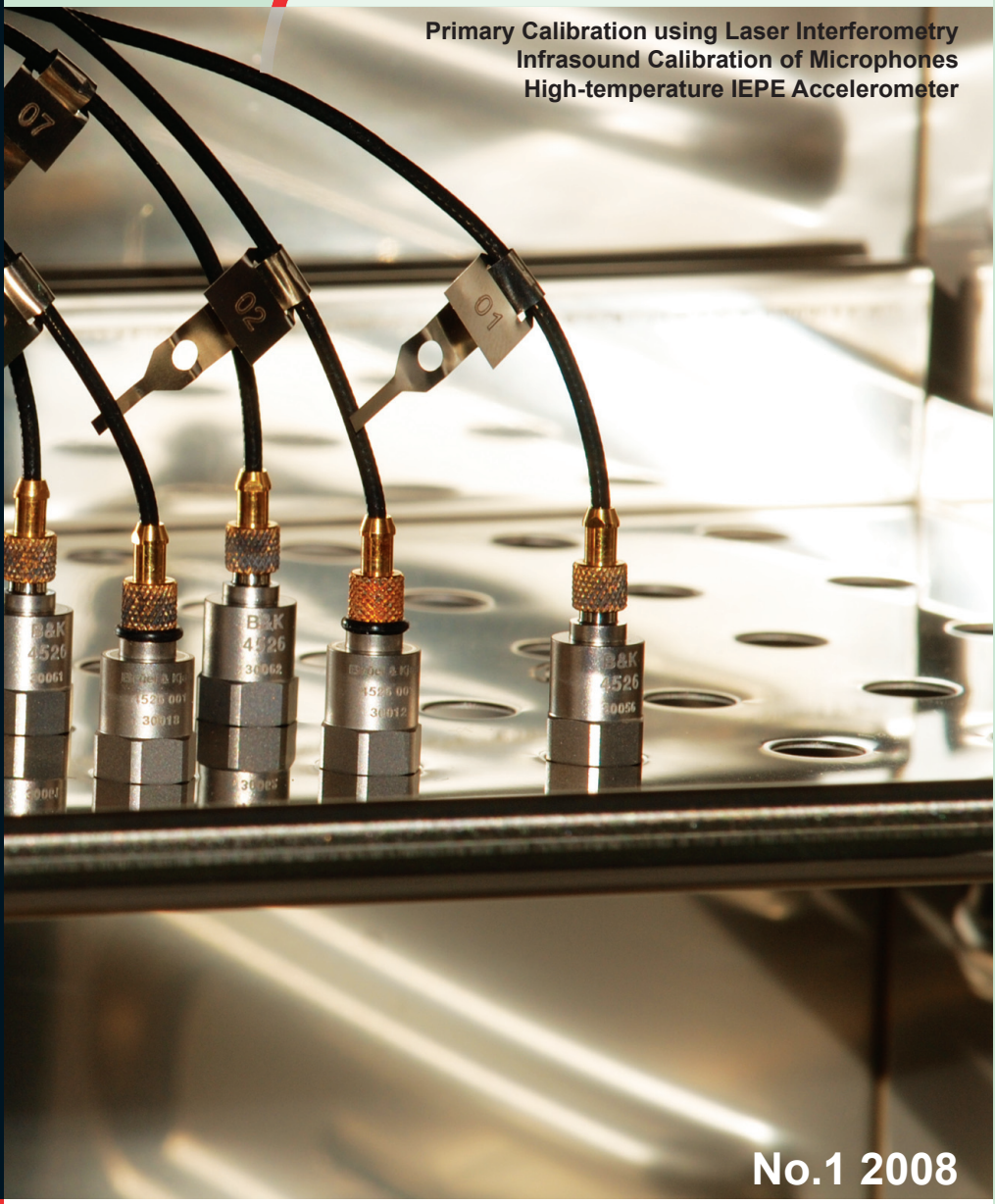

No.1 2008

Brüel & Kjær

Previously issued numbers of Brüel & Kjær Technical Review

1 – 2007 Measurement of the Normal Incidence Transmission Loss and Other Acoustical Properties of Materials Placed in a Standing Wave Tube

1 – 2006 Dyn-X Technology: 160 dB in One Input Range
Order Tracking in Vibro-acoustic Measurements: A Novel Approach Eliminating the Tacho Probe
Comparison of Acoustic Holography Methods for Surface Velocity Determination on a Vibrating Panel

1 – 2005 Acoustical Solutions in the Design of a Measurement Microphone for Surface Mounting
Combined NAH and Beamforming Using the Same Array
Patch Near-field Acoustical Holography Using a New Statistically Optimal Method

1 – 2004 Beamforming

1 – 2002 A New Design Principle for Triaxial Piezoelectric Accelerometers
Use of FE Models in the Optimisation of Accelerometer Designs
System for Measurement of Microphone Distortion and Linearity from Medium to Very High Levels

1 – 2001 The Influence of Environmental Conditions on the Pressure Sensitivity of Measurement Microphones
Reduction of Heat Conduction Error in Microphone Pressure Reciprocity Calibration
Frequency Response for Measurement Microphones – a Question of Confidence
Measurement of Microphone Random-incidence and Pressure-field Responses and Determination of their Uncertainties

1 – 2000 Non-stationary STSF

1 – 1999 Characteristics of the vold-Kalman Order Tracking Filter

1 – 1998 Danish Primary Laboratory of Acoustics (DPLA) as Part of the National Metrology Organisation
Pressure Reciprocity Calibration – Instrumentation, Results and Uncertainty
MP.EXE, a Calculation Program for Pressure Reciprocity Calibration of Microphones

1 – 1997 A New Design Principle for Triaxial Piezoelectric Accelerometers
A Simple QC Test for Knock Sensors
Torsional Operational Deflection Shapes (TODS) Measurements

2 – 1996 Non-stationary Signal Analysis using Wavelet Transform, Short-time Fourier Transform and Wigner-Ville Distribution

1 – 1996 Calibration Uncertainties & Distortion of Microphones.
Wide Band Intensity Probe. Accelerometer Mounted Resonance Test

2 – 1995 Order Tracking Analysis

1 – 1995 Use of Spatial Transformation of Sound Fields (STSF) Techniques in the Automative Industry

(Continued on cover page 3)

Technical Review

No. 1 – 2008

Table of Contents

ISO 16063–11: Primary Vibration Calibration by Laser Interferometry: Evaluation of Sine Approximation Realised by FFT 1
Torben R. Licht and Sven Erik Salbøl

Infrasound Calibration of Measurement Microphones 15
Erling Frederiksen

Improved Temperature Specifications for Transducers with Built-in Electronics 29
Lars Munch Kofoed and Morten Kirkelund

TRADEMARKS

DeltaShear is a registered trademark and PULSE is a trademark of Brüel & Kjær Sound and Vibration Measurement A/S
Microsoft is a registered trademark of Microsoft Corporation in the United States and/or other countries
ANSYS is a registered trademark of ANSYS, Inc.
ENDEVCO is a registered trademark of ENDEVCO Corporation

Editor: Harry K. Zaveri

ISO 16063–11: Primary Vibration Calibration by Laser Interferometry: Evaluation of Sine Approximation Realised by FFT*

Torben R. Licht and Sven Erik Salbøl†

Abstract

Laser interferometry – using counters for fringe counting and determination of zeroes at higher frequencies – has been used for accelerometer calibration since the late 1960s. As digital techniques evolved during the 1980s and 90s, it became possible to make a more sophisticated approach towards interferometer detectors' complex output signals. This evolution was described in a revision of the previous standard, ISO 5347–1, which resulted in the new ISO 16063–11 in 1999. In the new standard, the sine approximation method was introduced. As the input is known to be a sine, a least square fitting of the results calculated from the interferometer output gives good results. The fitting is essentially a filtering at the known frequency. Therefore, with the advanced high-resolution FFT analysers available today, it is logical to use such analysers to do the filtering.

A system following these concepts has been realised. This system will be described, and an evaluation of the system's sensitivity to different imperfections (e.g., noise and gain differences in the interferometer output) will be reported. The evaluation is made using computer-generated test signals, and the technique can also be used to verify the system whenever needed.

Résumé

Les interféromètres laser pour le comptage des franges et la détermination des zéros aux fréquences élevées sont utilisés pour l'étalonnage des accéléromètres

* First printed at XVIII IMEKO World Congress, Rio de Janeiro, Brazil, 2006.
† Both Authors: DPLA and Brüel & Kjaer S&V, Naerum, Denmark

depuis la fin des années soixante. Avec le développement du numérique dans les années 80 et 90, il est devenu possible d'utiliser des dispositifs plus évolués pour détecter par interférométrie des signaux de sortie complexes. Cette évolution a été décrite à l'occasion d'une révision de la Norme ISO 5347–1, qui a résulté en une nouvelle norme, ISO 16063–11, en 1999. Ce nouveau référentiel introduit la méthode par approximation d'une vibration sinusoïdale. Lorsqu'on sait que le signal en entrée est sinusoïdal, une approximation par la méthode des moindres carrés des résultats calculés en sortie par l'interféromètre donne de bons résultats. Comme l'opération peut essentiellement se résumer à un filtrage à une fréquence connue, il est logique d'utiliser pour ce faire les analyseurs FFT haute résolution disponibles aujourd'hui.

Un système a été mis au point sur la base de ces concepts. Il est décrit ici, ainsi qu'une évaluation de sa sensibilité à diverses imperfections (notamment les différences de gain et de bruit à la sortie de l'interféromètre). Cette évaluation repose sur des signaux d'essais générés par ordinateur, une technique qui peut aussi être utilisée pour vérifier le bon fonctionnement du système en cas de besoin.

Zusammenfassung

Laserinterferometrie – mit Zählern für Fringe Counting und die Erfassung von Nulldurchgängen bei höheren Frequenzen – wird seit Ende der 1960er Jahre bei der Kalibrierung von Beschleunigungsaufnehmern eingesetzt. Mit der Entwicklung der digitalen Techniken in den 1980er und 90er Jahren wurde eine ausgefeiltere Herangehensweise an die komplexen Ausgangssignale der Interferometerdetektoren möglich. Diese Entwicklung wurde in einer Überarbeitung der früheren Norm ISO 5347–1 beschrieben und resultierte 1999 in der neuen ISO 16063–11. In der neuen Norm wurde das Sinusausgleichsverfahren eingeführt. Da ein sinusförmiges Eingangssignal vorliegt, ergibt die Anpassung nach der Methode der kleinsten Quadrate gute Resultate für die aus dem Ausgangssignal des Interferometers berechneten Ergebnisse. Die Anpassung besteht hauptsächlich aus einer Filterung bei der bekannten Frequenz. Mit der hohen Auflösung der heute erhältlichen FFT-Analysatoren ist es naheliegend, die Filterung mit solchen Analysatoren vorzunehmen.

Es wurde ein System eingerichtet, das diesen Konzepten entspricht. Dieses System wird beschrieben und seine Anfälligkeit gegenüber verschiedenen Störfaktoren (z.B. Störkomponenten und Verstärkungsunterschiede im

Ausgangssignal des Interferometers) bewertet. Die Bewertung erfolgt anhand von computergenerierten Testsignalen. Diese Technik lässt sich auch verwenden, um das System bei Bedarf zu überprüfen.

Introduction

An example of a classical laser interferometric setup is shown in Fig. 1.

Fig. 1. Classic laser interferometric setup

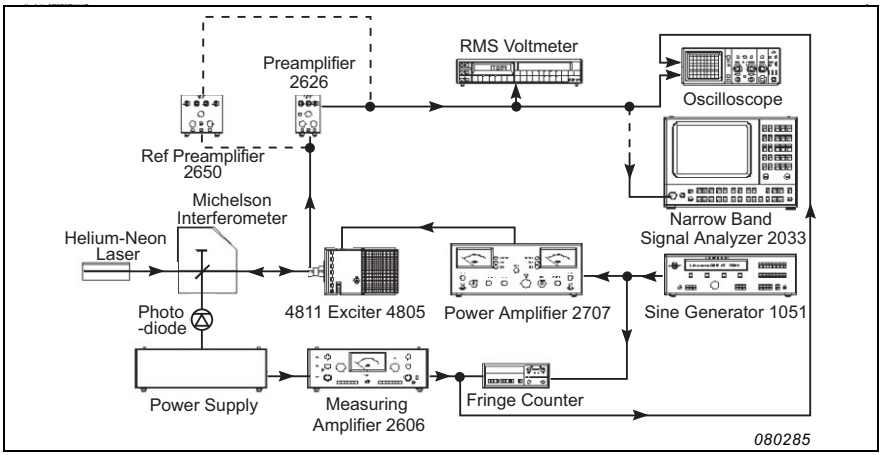

Fig. 2 shows the basic fringe counting, or ratio principle. Equations 1a through 1d show the calculations needed to find the acceleration.

$$\text{vibration } x(t) = \hat{d}\sin(\omega t + \varphi) \tag{1a}$$

$$R_f = (8\hat{d})/\lambda \tag{1b}$$

$$\hat{a} = \hat{d}\omega^2 \tag{1c}$$

$$R_f = \frac{8\hat{a}}{\omega^2\lambda} = \frac{8a_{\text{rms}}\sqrt{2}}{(2\pi f)^2\lambda} \tag{1d}$$

Example: Given the above equations, if $a_{\text{rms}} = 50\,\text{ms}^{-2}$ and $f = 159.155\,\text{Hz}$ ($\omega = 1000$), then $R_f = 893.92$.

Fig. 2. Fringe counting

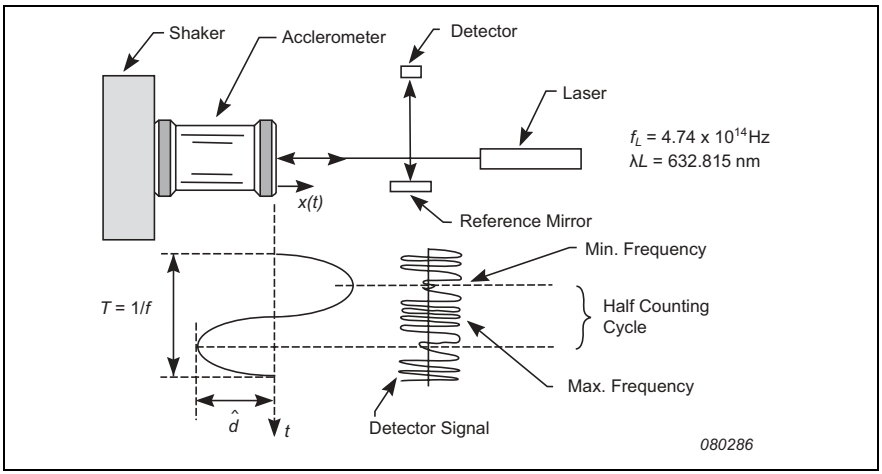

Fig. 3. New setup with quadrature output

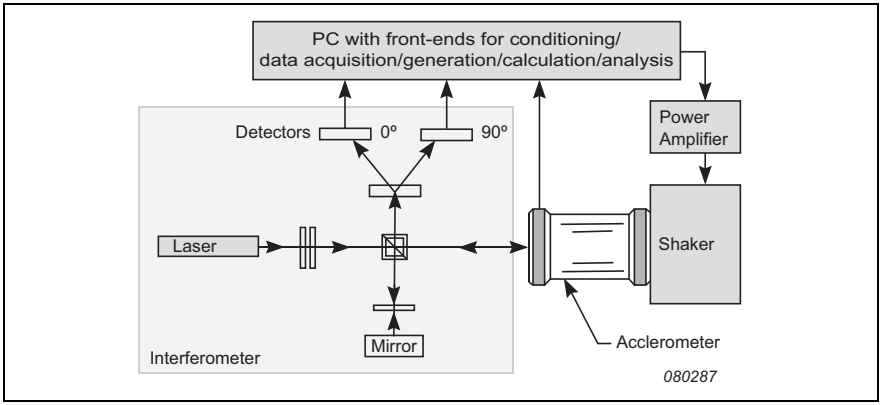

Fig. 3 shows the principle of more recent systems. The interferometer, which can be an integrated unit or a setup as shown, provides two outputs in quadrature.

These signals and the signal from the accelerometer are all conditioned by suitable preamplifiers if necessary and then digitized. The output for generation of the vibration through the power amplifier and shaker is also generated digitally and then converted to an analog output signal. The same clock controls all digitizing. The PC is the heart of all these functions and controls the system.

ISO 16063–11:
Primary Vibration Calibration by Laser Interferometry

The most commonly used method in systems, as the one sketched in Fig. 2 is Method 3, sine approximation as described in ISO 16063─11:1999 [1].

This method results in a discrete time series of modulation phase values calculated from the digitized detector outputs $u_1(t_i)$ and $u_2(t_i)$ using the relationship:

$$\varphi_{\text{Mod}}(t_i) = \arctan\frac{u_2(t_i)}{u_1(t_i)} + p\pi \tag{2}$$

where the integer p must be chosen properly in order to avoid discontinuities.

These results are then used to create $N+1$ equations, such as

$$\varphi_{\text{Mod}}(t_i) = A\cos\omega t_i - B\sin\omega t_i + C \tag{3}$$

to be solved using the least squares method to find A, B and C, where

$i = 0,1,2...N$

$A = \varphi_M \cos\varphi_s$

$B = \varphi_M \sin\varphi_s$

C is a constant

ω is the angular frequency of vibration $\omega = 2\pi f$

φ_s is the initial phase of the displacement

$N+1$ is the number of samples taken synchronously over the measurement period

f is the vibration frequency known by the system

If we look at the Discrete Fourier Transformation (DFT) of any time series of $N+1$ elements taken over a time $T = 1/f$, this can be described by

$$\varphi_{\text{Mod–DFT}}(t_i) = C' + \sum_{n=1}^{N} \hat{\varphi}_{Mn} \cos\left(n\omega t_i + \varphi'_s\right) \tag{4}$$

$$= C' + \sum_{n=1}^{N} \hat{\varphi}_{Mn} (\cos \varphi'_s \cos n\omega t_i - \sin\varphi'_s \sin n\omega t_i)$$

$$= C' + A' \cos \omega t_i - B' \sin \omega t_i$$

$$+ \sum_{n=2}^{N} \hat{\varphi}_{Mn} (\cos \varphi'_s \cos n\omega t_i - \sin\varphi'_s \sin n\omega t_i)$$

The least squares method requires minimizing:

$$\sum_{i=1}^{N} \left(\varphi_{\text{Mod–DFT}}(t_i) - \varphi_{\text{Mod}}(t_i)\right)^2 \tag{5}$$

$$= \sum_{i=1}^{N} \left(\begin{array}{l} C' + A' \cos \omega t_i - B' \sin \omega t_i \\ + \sum_{n=2}^{N} \hat{\varphi}_{Mn} (\cos \varphi'_s \cos n\omega t_i - \sin\varphi'_s \sin n\omega t_i) \\ -(C + A \cos \omega t_i - B \sin \omega t_i) \end{array} \right)^2$$

and if we set $\hat{\varphi}_{M1} = \hat{\varphi}_M$, $\varphi'_s = \varphi_s$ such that $A' = A$, $B' = B$, $C' = C$, then:

$$\sum_{i=1}^{N} (\varphi_{\text{Mod–DFT}}(t_i) - \varphi_{\text{Mod}}(t_i))^2 \tag{6}$$
$$= \sum_{i=1}^{N} \left(\sum_{n=2}^{N} \hat{\varphi}_{Mn} (\cos \varphi_s \cos n\omega t_i - \sin \varphi_s \sin n\omega t_i) \right)^2$$
$$= \sum_{i=1}^{N} \left(\sum_{n=2}^{N} \hat{\varphi}_{Mn} (\cos (n\omega t_i + \varphi_s)) \right)^2$$

which becomes equal to zero if all $\hat{\varphi}_{Mn}$ for $n \geq 2$ are zero. This means that only the fundamental frequency is left, and all harmonics are rejected, as would be expected. If m times longer records are used, the vibration frequency will just be the m^{th} harmonic (m being an integer ≥ 2).

Thus it is proved that, with appropriate sampling and removal of values for the proper frequency, using DFT (or the faster FFT) is identical to the described sine approximation method.

The Role of FFT Analyzers

Using standard FFT analyzers and selecting vibration frequencies and settings of the analyzer in such a way that the vibration frequency coincides with a centre frequency of one of the frequency bands (which is the same as requiring the record length to be a multiple of the period of the vibration frequency) will give exactly the same results as described above (independent of any time window used).

However, it is desirable to permit the free choice of frequencies. Therefore, a special flat-top time window can be used in FFT analysis. This requires a somewhat longer time record but will give the correct parameters for the vibration frequency component – within 0.03% for frequencies less than 0.43 times the frequency resolution used for analysis from the centre frequency and maximum 0.113% off at the worst point in the middle between two analysis bands. The response of such a filter is shown in Fig. 4, where the values for the distance from the frequency to the centre frequency of a band is normalized by the frequency resolution df. The flat-top time window is shown in Fig. 5.

This means that we can use a high-resolution calibrated analyzer to measure the ratio between the displacement calculated from the laser signals and the accelerometer output, and still get very high accuracy. Even in the worst case,

Fig. 4. Flat-top filter characteristics

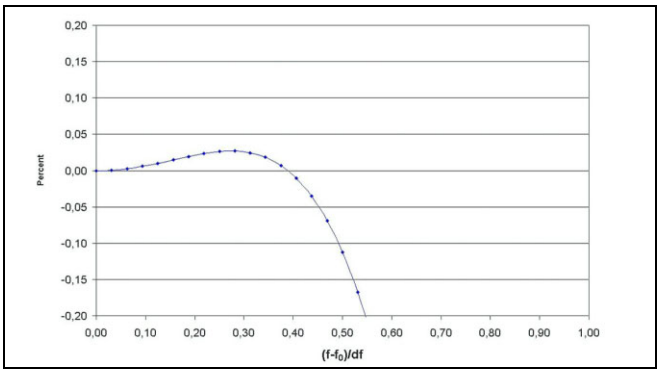

Fig. 5. Flat-top time window

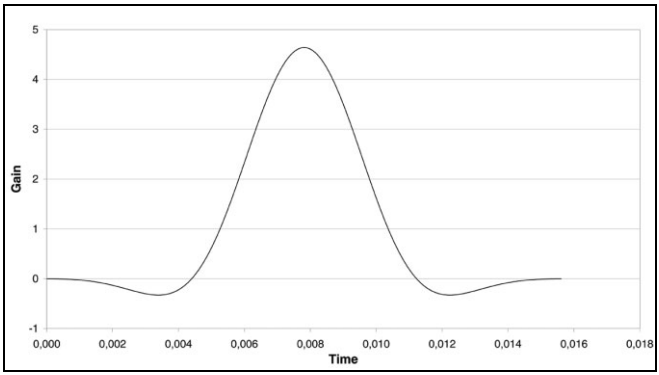

which can be avoided, it will only contribute 0.1%. If the same filter is used in both channels, only the difference contributes, giving less than 0.01% error. A correction is also possible.

Analyzer calibration can be performed in different ways. One method that fits well with the procedures in many laboratories is to base the calibration on a high-precision digital multimeter (DMM). This can give accuracies on the order of 0.03 to 0.1% ($2\,\sigma$ values) above 10 Hz and about twice these values below 10 Hz. Automating the calibration and storing the results in a database facilitates the automatic correction of the measurements, which allows the future transferrence of the DMM accuracies to the analyzer nearly without any increase in uncertainty. This method can also provide traceability.

The voltmeter used to calibrate the analyzer is in a sampling mode below 2 Hz. This is necessary as the voltmeters are not very accurate for normal AC measurements below 2 Hz.

Example of Implementation

A system following the ideas outlined above has been implemented. The block diagram in Fig. 6 shows the data flow through the system, based on a Brüel & Kjaer analyzer in the PULSE family.

Fig. 6. Laser Calibration System using PULSE FFT Analyzer

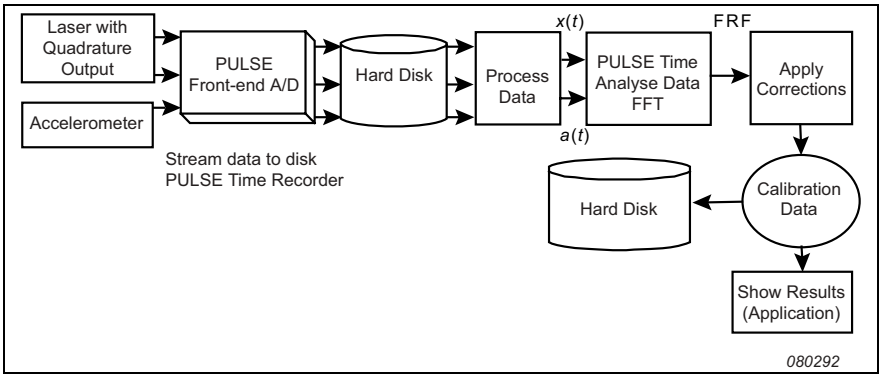

The initial operation is an A/D conversion (16 bit) and recording of raw data from the two detectors in quadrature and the accelerometer onto the hard disk. The maximum sample rate is used, and all channels are sampling synchronously to ensure that the phase relationships are kept. Streaming the data directly to the hard disk makes it unimportant how large the files are but naturally large amounts of data take longer to process. This permits, for example, measurements at very low frequencies, down to 0.1 Hz, producing files of several hundred Megabytes each.

When the recording of data at each of the desired frequencies is finished, the data from the laser are processed and stored as UFF files together with the data from the accelerometer. After finishing all frequencies, these files ($x(t)$ and $a(t)$) are then sequentially read back into the PULSE Time Analyzer, as files, not through analyzer hardware. Here the FFT analyzer treats the signals and sends the results to the calibration software, which applies any final corrections (from the DMM data) and sends the results to the hard disk and the display. Measurement examples are shown in Fig. 7 and Fig. 8.

Fig. 7. Wide-range calibration of reference in shaker (2 Hz to 50 kHz; Magnitude and Phase)

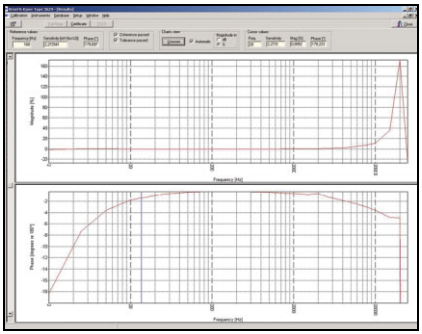

Fig. 8. Calibration of servo accelerometer on a long-stroke shaker (0.1 to 160 Hz;0.2% /division)

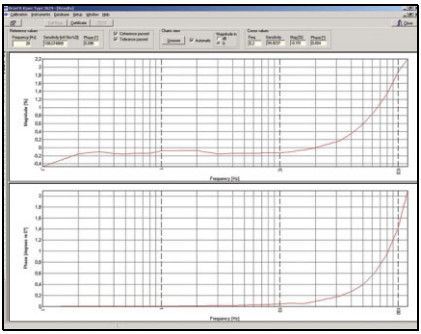

Problems and Requirements

A problem for laser interferometry occurs at high frequencies – typically above 1 kHz. The calculation of the $\varphi_{\mathrm{Mod}}(t_i)$ values can graphically be explained as shown in Fig. 9. Ideally the two laser detector outputs describe a circle if plotted one on each of two perpendicular axes. However, in practice two requirements have to be fulfilled before calculations can be made.

The first requirement is that the circle does not degenerate into an ellipse, corresponding to different sensitivities or intensities in the two channels. This can be corrected by normalizing the two signals.

The next requirement is that a centre can be determined for the circle. When the displacement in the motion becomes less than about half a wavelength, a full circle is no longer described, and the centre becomes increasingly difficult to find. This scenario results in an increase of uncertainties.

This scenario is avoided by using the dual tone feature of the analyzer. By adding a suitable signal at a low frequency, typically in the 100 to 200 Hz range, a full circle is formed, and the high-frequency motion is now a kind of modulation on top of the smooth motion of the point on the circle. When the analysis is performed afterwards, it only means that we can find a signal at this frequency, far away from the frequency of interest, which does not interfere with the measurement.

Evaluation of Influences

Due to the modularity of the system, it is possible to test the influence of different parameters in data treatment and analysis. Raw data can be generated and stored just as data from the PULSE front-end are stored. The system can use these data

Fig. 9. Determination of the Mod angle

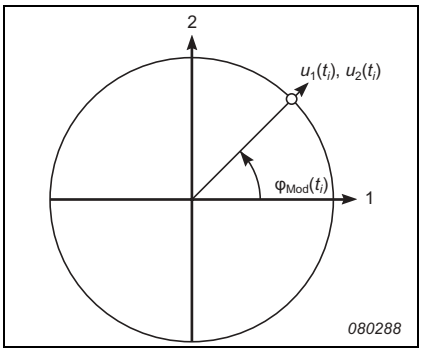

Fig. 10. Simulation result with 0.8 ellipticity

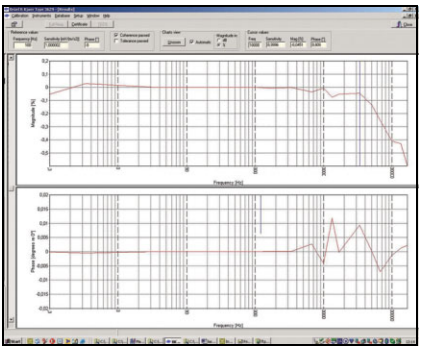

and give results just as for normal calibrations. Fig. 10 shows an example result. The raw data are generated by means of a mathematical model in Mathcad, containing both the fundamental calculus and noise on detectors and accelerometer and an ellipticity between the two channels. The scales are 0.1%/division and 0.005º/division.

Fig. 11. Amplitude deviation result of simulation with 0.8 and 1 ellipticity

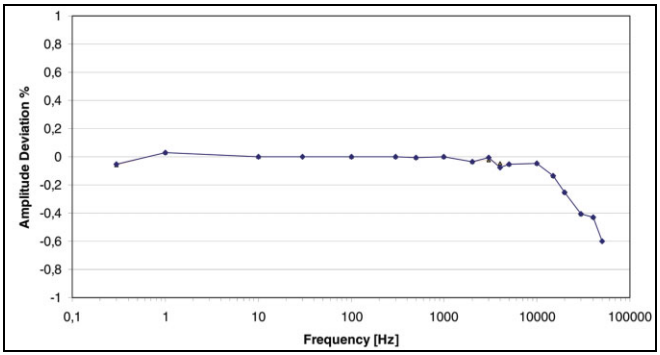

Fig. 11 and Fig. 12 show results from tests with an ellipticity of 1 and 0.8. The magnitude variation over the frequency range of 0.3 to 3000 Hz is less than 0.05%, less than 0.1% to 10 kHz and remains below 0.6% up to 50 kHz. The phase deviations remain below 0.01º over the full frequency range – as shown in Fig. 12. Fig. 13 shows the difference in the obtained percentage variations on the magnitudes for 0.8 and 1 ellipticity. The difference remains below 0.03% from

Fig. 12. Phase deviation result of simulation with 0.8 and 1 ellipticity

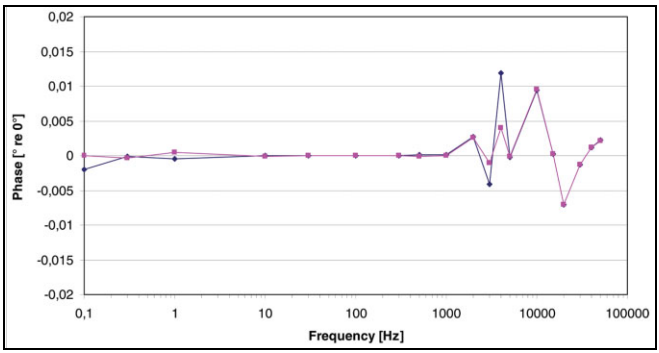

Fig. 13. Amplitude deviation difference in percentage simulation results with 0.8 and 1 ellipticity

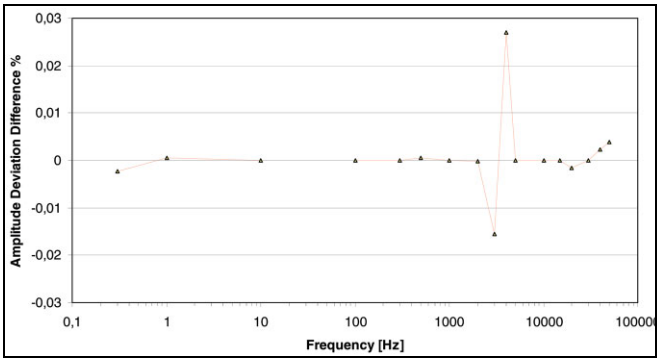

0.3 Hz to 50 kHz. The calculated sensitivities at the reference frequency were all within ±0.0002% from the expected value.

Conclusion

It has been proved that a system based on modern analyzers is well suited to perform primary calibrations following ISO 16063–11, Method 3.

The influence on the total measured sensitivity magnitude from typical noise and ellipticity variations has been shown to be less than 0.1% over the frequency range of 0.3 Hz to 10 kHz and less than 0.6% up to 50 kHz.

The influence on the total measured sensitivity phase from typical noise and ellipticity variations has been shown to be less than 0.001º over the frequency range of 0.3 Hz to 1 kHz and less than 0.01º up to 50 kHz.

Reference

[1] ISO 16063–11:1999. *Methods for Calibration of Vibration and Shock Transducers – Part 11*: *Primary Vibration Calibration by Laser Interferometry*. ISO 1999

Infrasound Calibration of Measurement Microphones

Erling Frederiksen[*]

Abstract

This paper describes methods and equipment for frequency response calibration of measurement microphones over the range of 0.1 to 250 Hz. New calibration principles are described together with a design for a new reference microphone and a dedicated low-frequency calibration unit. Expected calibration uncertainties are also stated. The motivation for the work behind the paper is the, presently, very high international interest in low-frequency microphone calibration that, among other activities, has initiated a BIPM key comparison project on the calibration of 1 inch Laboratory Standard Microphones down to 2 Hz.

Résumé

Cette communication décrit les méthodes et l'appareillage utilisés pour l'étalonnage de la réponse en fréquence des microphones de mesure dans la gamme comprise entre 0,1 et 250 Hz. Y sont présentés de nouveaux principes d'étalonnage, une nouvelle conception du microphone de référence et une instrumentation dédiée pour l'étalonnage basse fréquence. Y sont également inventoriées les valeurs d'incertitude. Ces travaux ont été motivés par le grand intérêt actuel, au plan international, concernant l'étalonnage des microphones de mesure basse fréquence. Un intérêt, qui, parmi d'autres initiatives, a entraîné la mise en route par le BIPM d'un projet de comparaison clé relatif au calibrage des microphones standard de laboratoire de 1 pouce jusqu'à des fréquences aussi basses que 2 Hz.

* DPLA and Brüel & Kjaer S&V, Naerum, Denmark

Zusammenfassung

Dieser Artikel beschreibt Methoden und Ausrüstung zur Frequenzgangkalibrierung von Messmikrofonen im Bereich von 0,1 bis 250 Hz. Es werden neue Kalibrierprinzipien beschrieben sowie eine Bauart für ein neues Bezugsmikrofon und eine spezielle Kalibriereinheit für tiefe Frequenzen. Die erwarteten Kalibrierunsicherheiten werden ebenfalls angegeben. Die diesem Artikel zugrundeliegenden Arbeiten wurden durch das gegenwärtig sehr starke internationale Interesse an tieffrequenter Mikrofonkalibrierung angeregt, das unter anderem einen BIPM Schlüsselvergleich zur Kalibrierung von 1-Zoll Laboratorium-Normalmikrofonen bis hinab zu 2 Hz veranlasst hat.

Introduction

Within the last decade, the interest in low-frequency microphone calibration has increased all over the world. This interest was expressed to the Bureau International des Poids et Measures (BIPM) who, therefore, initiated a key comparison calibration project with the title 'Comparison of Laboratory Standard Microphone Calibrations at Low Frequencies'. One-inch microphones (IEC 61094–1 LS1) are to be calibrated from 2 to 250 Hz. The project is running with participation from national metrology institutes. As most participants apply the reciprocity technique, the project is also very interesting for the International Electrotechnical Commission (IEC), who are presently revising the pressure calibration standard, IEC 61094–2, to extend the frequency range down to 2 Hz. This paper describes a part of the work performed by the Danish Primary Laboratory of Acoustics (DPLA). The substance of this paper is to examine other methods that might verify the reciprocity results and partly to develop a system of low-frequency calibration for all types of measurement microphones. This system should preferably work down to 0.1 Hz.

Operation Modes and Low-frequency Responses

Most measurement microphones are pressure-sensing condenser microphones; i.e., their diaphragms respond to the pressure difference between their front and rear sides. The rear side pressure is the pressure in an air-filled cavity behind the diaphragm. Because static pressure variation may be very large over time, it could overload and destroy the functionality of the microphone. Therefore, static pressure must be equalized with the ambient pressure. The cavity must have a vent

that equalizes static pressure, but prevents equalization of sound pressure at the lowest frequencies of interest.

Frequency response depends on the way in which the microphone is exposed to the sound pressure. If only its diaphragm is exposed, the response is essentially flat to DC, but if both diaphragm and vent are exposed, it rolls off at low frequencies. The frequency of the '–3 dB-point' is called the lower limiting frequency. For most microphones, the lower limiting frequency is between 1 and 3 Hz – but lower for dedicated low-frequency microphones (see Fig. 1 and Fig. 2). The flat response is the microphone pressure response, which is defined for exposure of the diaphragm only. When applied for measurements in free or diffuse sound fields, the microphone is fully surrounded by the sound; therefore, the vent is also exposed, and the free- and diffuse-field responses roll off.

Fig. 1. Diaphragm only (left) – relates to pressure response
Both diaphragm and vent (right) – relates to the free- and diffuse-field responses

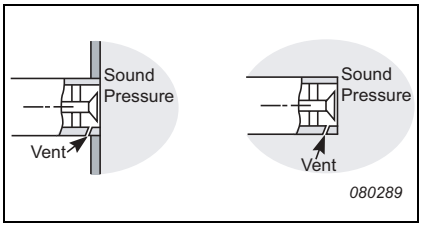

Fig. 2. Pressure response (solid curve) and free- and diffuse-field response (dashed curve) Brüel & Kjær microphone Type 4190

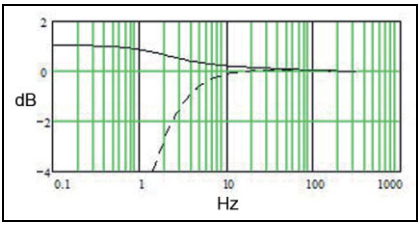

The lumped parameter model (see Fig. 3) shows the elements that determine the low-frequency response and sensitivity of a microphone. As in a real field, pressure can be applied in two ways. The pressure response is simulated by applying the input signal between the diaphragm terminal (T_d) and the ground terminal (T_0), while the terminal of the equalization vent (T_v) is connected to ground (T_0). The equal free- and diffuse-field responses are simulated by applying the signal to both diaphragm and vent (T_d and T_v). The impedance of the internal microphone cavity is simulated by the (adiabatic) compliance of the internal volume (C_{vo}) and by the 'R' and 'C' elements marked h1, h2, … , h5. They represent the effect of heat conduction – exchange of heat between the compressed/decompressed air and the solid cavity surfaces.

The model leads to the following equations for calculation of pressure (Eq. 1) and the free- and diffuse-field (Eq. 2) sensitivity as a function of frequency:

Fig. 3. Low-frequency model of a typical condenser microphone

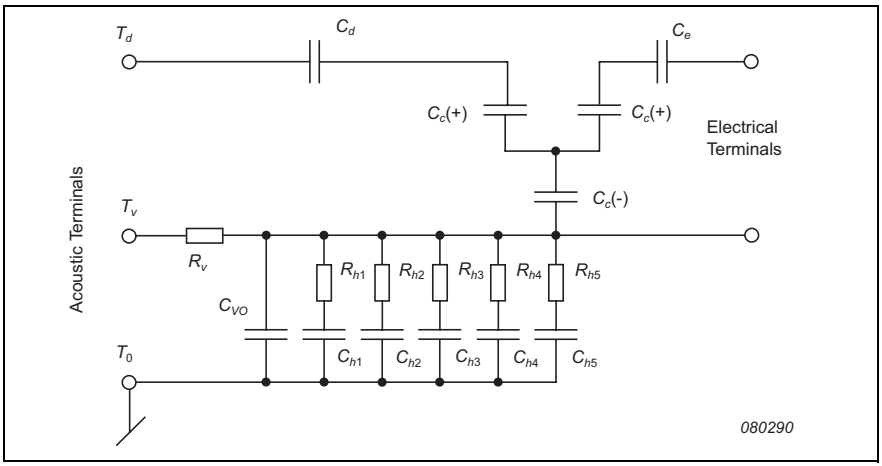

$$M_p(f) = \frac{Z_c}{Z_d + \dfrac{Z_{cav} \cdot R_v}{Z_{cav} + R_v}} \tag{1}$$

$$M_{fd}(f) = \frac{Z_c}{Z_d + \dfrac{Z_{cav} \cdot R_v}{Z_{cav} + R_v}} - \frac{\dfrac{Z_{cav} \cdot Z_d}{Z_{cav} + Z_d}}{\dfrac{Z_{cav} \cdot Z_d}{Z_{cav} + Z_d} + R_v} \cdot \frac{C_d}{C_c} \tag{2}$$

where:

$M_p(f)$ is microphone pressure sensitivity (V/Pa)
$M_{fd}(f)$ is microphone free-/diffuse-field sensitivity (V/Pa)
C_c is electro-mechanical coupling compliance of microphone* (m^3/V)
C_d is microphone diaphragm compliance (m^3/Pa)

* '+' and '–' signs of C_c indicate positive and negative element values, whose absolute values are equal

R_v is microphone vent resistance (Pa·s/m^3)
Z_c is coupling compliance impedance, $(j \cdot 2\pi f C_c)^{-1}$, (Pa·s/m^3)
Z_d is diaphragm compliance impedance, $(j \cdot 2\pi f C_d)^{-1}$, (Pa·s/m^3)
Z_{cav} is rear cavity impedance (see equivalent circuit):
C_{vo} is rear cavity volume compliance (m^3/Pa)
$C_{h\#}$ is additional compliance due to heat conduction (m^3/Pa)
$R_{h\#}$ is element of loss due to heat conduction (Pa·s/m^3)

In this project and for this paper, the model has been applied for creating frequency response graphs and, more important, for testing Equation 3 that was worked out for determining the frequency response of the reference microphone, described in the next section.

Frequency Response Calibration

The primary pressure reciprocity calibration method (IEC 61094–2) yields the pressure response of the calibrated microphones (IEC 61094–1 LS1 and LS2). Therefore, further steps have to be taken to determine free- or diffuse-field responses of these and other microphones. In fact, due to the low ratio between the microphone dimensions and the wavelength of the sound, there is no difference between the free- and the diffuse-field response of a microphone at the low frequencies that are dealt with in this paper ($f < 250$ Hz). For the same reason, neither a free nor a diffuse sound field is necessary for low-frequency calibration – only the proper sound exposure of diaphragms and vents is important. It is thus possible to perform calibrations of free- and diffuse-field responses by using the pressure field of a comparison coupler. The unknown microphones should in this case be fully inserted in its cavity, while the reference microphone, which is generally pressure response calibrated, should be placed in the coupler wall with its vent opening outside the cavity, see Fig. 4.

In the low-frequency range ($f < 20$ Hz), the well-established reciprocity calibration method has some practical and theoretical weaknesses, such as a less elaborate theory on coupler and microphone impedance, and problems with leakage of couplers. For these reasons and because of the lack of a method for the 0.1 to 2 Hz range, other methods were invented and considered for this project, see below.

These methods are not absolute methods, but relative methods. They can be used for determining frequency response level reletive to the sensitivity level at a selected frequency. Absolute sensitivities can be obtained by combining one of the

Fig. 4. Mountings for calibration of pressure (left) and free- and diffuse-field responses (right)

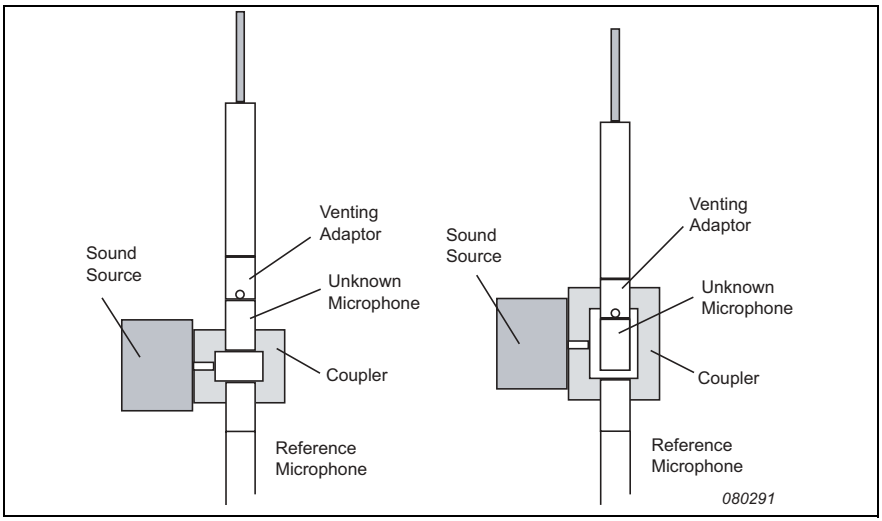

methods with an absolute calibration at the reference frequency. The selected reference frequency should be a frequency at which the absolute sensitivity can be determined with low uncertainty.

Design of Low-frequency Reference Microphone

In principle, any type of stable condenser measurement microphone that can be precisely pressure calibrated could be applied as the reference standard of a low-frequency comparison calibration system. However, a specific half-inch microphone was made for the project. Compared to similar measurement microphones, this has a higher diaphragm tension and larger internal cavity (see Fig. 5). This leads to a lower fraction of air-stiffness and, therefore, to an essentially flat pressure frequency response. This varies by less than 0.2 dB over the range between 0.1 and 250 Hz, see Fig. 6. The stiff diaphragm also reduces the effect of static pressure variations on the microphone sensitivity. This is important as minor, but disturbing, pressure changes may easily arise inside the low-frequency couplers and inside the microphone cavities. The changes may occur due to the electrical heating of the source and the preamplifiers in combination with the relatively long pressure equalization time constants of the couplers.

Fig. 5. New low-frequency reference micropnone (right) and common measurement microphone (left)

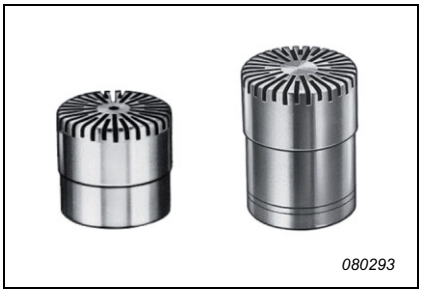

Fig. 6. The pressure response of the low-frequency reference microphone

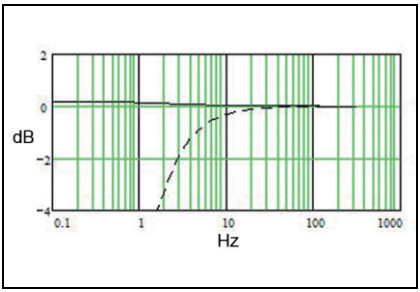

Furthermore, this low-sensitivity (–43.5 dB re 1 V/Pa) half-inch microphone is designed with same housing and geometry of its internal cavity as that of the much more sensitive (–26 dB re 1 V/Pa) standard type of microphone Brüel & Kjær Type 4190. This means that large batches of Type 4190 microphones are available for selecting a unit that matches the dedicated reference microphone on venting resistance and that it, therefore, becomes easy to form a pair of microphones that is well suited for use with the Related Microphones Method described on page 22.

Calibration of Reference Microphone

Electrostatic Actuator Method

Electrostatic actuators are, in principle, ideal tools for low-frequency pressure response calibration as their simulated sound pressure is frequency-independent, if the driving AC-voltage is kept constant. However, as neither the driving instruments nor the applied analyzer have fully flat frequency responses, the measured responses must be corrected for the response of the measurement system itself. This is not easily done, because the actuator voltage is far too high to be led to the microphone input terminals. It is not easy to obtain a frequency-independent attenuation of about 70 dB (about 3000 times) with a circuit that can withstand 100 V AC and 800 V DC and that does not load the amplifier output significantly.

This led to the idea of measuring the system response without making any changes of the normal actuator measurement setup, but by placing the microphone in vacuum, where its low-frequency response is essentially flat and thus without

influence on the system response. The pressure should just be about 5 kPa (or lower) to ensure that the response of the above reference microphone is flat within 0.01 dB.

This method was evaluated and was expected to give very precise calibration results, with uncertainties less than 0.05 dB. This expectation is still valid, but the experiments failed, because the vacuum equipment that was available did not have a static pressure stability that was high enough for performing repeatable measurements down to low frequencies. With the Brüel & Kjær PULSE Analyzer and the steady state response (SSR) software it takes about 30 minutes to measure frequency response in 1/3-octave steps from 250 to 0.1 Hz (standard deviation 0.01 dB).

Calibration laboratories with suitable vacuum systems are encouraged to test the method and report their results.

Related Microphones Method

This method of low-frequency response calibration requires two microphones of related designs. The dimensions of the internal cavities and the resistance of their static pressure equalization vents should be equal. Ideally, the microphones should only differ on the tension of their diaphragms. If these requirements are fulfilled, the frequency response of the less sensitive microphone can be determined by measuring 1) ratios of frequency response, 2) average sensitivity and 3) capacitance of the two microphones and by performing a calculation in accordance with Equation 3:

$$\left(\frac{M_2(f)}{M_2(f_{\text{ref}})}\right)_{\text{estim}} \cong \left(\frac{M_1(f)}{M_1(f_{\text{ref}})} \cdot \frac{M_2(f_{\text{ref}})}{M_2(f)} - 1\right) \cdot \left(\frac{M_{a,1}}{M_{a,2}} \cdot \frac{C_{ac,2}}{C_{ac,1}} - 1\right)^{-1} + 1 \qquad (3)$$

where:

$\left(\frac{M_2(f)}{M_2(f_{\text{ref}})}\right)_{\text{estim}}$ is the estimated normalised frequency response of the less sensitive microphone (2)

$\frac{M_1(f)}{M_1(f_{\text{ref}})} \cdot \frac{M_2(f_{\text{ref}})}{M_2(f)}$ is the measured ratio of normalised frequency responses of the related microphones (1) and (2)

f_{ref} is normalization frequency (250 Hz)

$M_{a,1}/M_{a,2}$ is the measured ratio between the average sensitivities of microphones (1) and (2)

$C_{ac,2}/C_{ac,1}$ is the measured ratio between the active capacitance of microphones (2) and (1). Passive microphone capacitance (typically between 1 and 3 pF) should be subtracted from the measured values.

The above equation is not exact. It is empirically determined, but it has been tested with the general low-frequency microphone model shown in Fig. 3 and has been found to be quite precise. The testing was made with two specific models of microphone, one of them corresponding to the specially designed low-frequency reference microphone and the other to a selected microphone Brüel & Kjær Type 4190, which meets the requirements of relation mentioned above. Fig. 7 shows the frequency responses calculated for the two microphones that have different diaphragm tension, but same impedance of their rear cavities. The figure also shows the calculated ratio, i.e., the difference in dB between the frequency responses, which, in practice, is easily measured for a real pair of microphones. Fig. 8 shows partly the estimated response of the less sensitive reference microphone obtained by using the above equation and partly the directly calculated response. Also the error of the estimation, i.e., the difference between the estimated and directly calculated responses, is shown. The error is less than 0.01 dB over the entire frequency range from 0.1 to 250 Hz with models of

Fig. 7. Calculated frequency responses of models of the reference microphone (lower solid curve) and of the related, more sensitive, microphone (upper solid curve). The dashed curve is the calculated difference

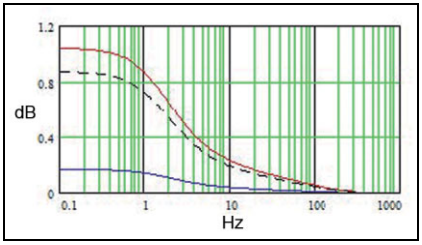

Fig. 8. Reference microphone model frequency responses. Directly calculated response (blue curve) with the response estimated from microphone response diferences in accordance with Eq. 3. Estimation error is also shown: Max. value is about 0.01 dB

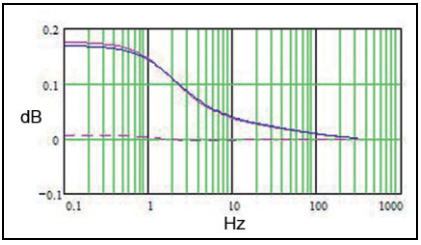

microphone that meet the mentioned requirements and have sensitivity of –26 dB and –43 dB re 1 V/Pa, respectively. This was found also to be the case for microphones with a rear cavity that differs much more from the applied model than the assumed uncertainty of this. In practice, it may be difficult to find a microphone that closely matches the reference microphone on the vent resistance, but a test has shown that the total error of the estimation equation is less than 0.01 dB if the vent resistances of the microphones differ by less than 10%.

The measured and normalized ratio between the responses of the two microphones is shown in Fig. 9 together with the response of the less sensitive microphone that is determined by Equation 3. The response varies slightly more than expected, but it is assumed to be within the tentatively estimated uncertainty that is stated in Table 1.

Fig. 9. Measured and normalized frequency response ratio (upper curve) used for estimation of the less sensitive microphone's frequency response (lower curve)

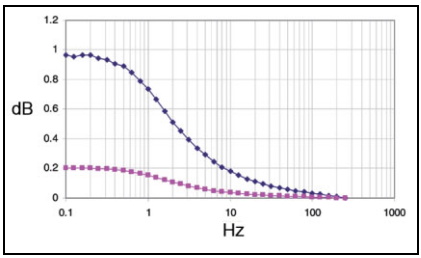

Table 1. Tentative estimated calibration uncertainty of reference microphone (k=2)

0.1 Hz	0.316 Hz	1 Hz	3.16 Hz	10 Hz	250 Hz
<0.05 dB	<0.05 dB	<0.04 dB	<0.03 dB	<0.02 dB	Ref.

After calibration, this microphone served as the reference microphone for the calibration of different types of microphones by using the comparison calibration unit described in the following section.

Low-frequency Comparison Calibration Coupler

One part of this project was design and calibration of a reference microphone that should be used with a comparison calibration unit for calibration of different types and sizes of microphone. Another part was the design of this unit that will briefly be described in the following. The unit operates over the range from 0.1 to 250 Hz.

Its built-in sound source is an ordinary loudspeaker with an airtight diaphragm. This works into a speaker cavity that, via sound channels, is connected to the cavity, where microphones are inserted in accordance with the sound exposure principles illustrated in Fig. 4. The design ensures that the sound pressure at the two microphones is the same – also at the highest frequency 250 Hz. The reference microphone is mounted at the lower side of the coupler, while the unknown microphone is inserted from above, see Fig. 10. Different adaptors were designed for proper sound exposure of calibrated microphones. Sometimes the microphone preamplifier influences the path along which the equalization takes place. In such cases, the adaptor should enclose both microphone and preamplifier. The volume of the adaptor cavity that loads the coupler is not critical. A cavity behind the loudspeaker diaphragm prevents sound emission to the ambient. The cavities in front of and behind the speaker are vented. The values of the vent resistances are selected as a compromise between flatness of frequency response and efficiency of the vents to equalize the minor, but disturbing, static pressure variations that may occur. They may originate from the ambient and/or be generated by the electrical power supplied to microphone preamplifiers and loudspeaker. The frequency response of the unit is generally flat, but it increases by about 3 dB at 250 Hz. The testing and the measurements were made at levels of 94 to 114 dB.

Fig. 10. Low-frequency calibration unit: 145 mm diameter

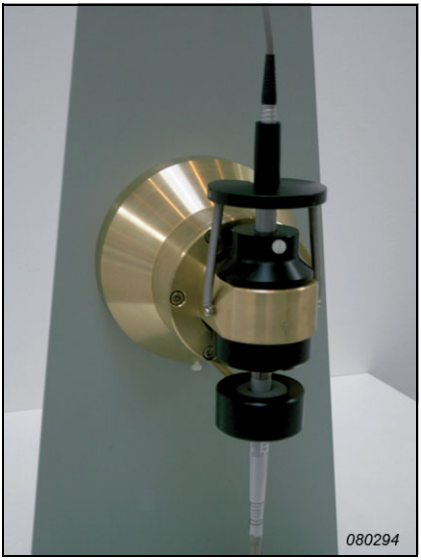

Conclusions

The activities behind this paper have resulted in a new low-frequency method for frequency response calibration, in a new reference microphone and in a practically applicable low-frequency calibration unit. As the frequency range, 0.1 to 250 Hz,

of the reference microphone and the calibration unit overlaps the audio range, the absolute sensitivity at low frequencies may be obtained by calibrating the reference microphone at an audio frequency, say at 250 Hz, where low uncertainty is easily obtained. Promising results have been obtained, but the activities will continue with further measurements that are expected to support the work of BIPM and IEC. The electrostatic actuator method called the vacuum method is another promising low-frequency calibration method.

Appendix: Notes on Calibration of Laboratory Standard Microphones by the Active Low-frequency Coupler

The Danish Primary Laboratory of Acoustics (specifically the Brüel & Kjaer portion) has invented a new method for frequency response calibration of infrasound reference microphones and designed a new active coupler for the purpose. In addition to the coupler, the method requires two identically shaped microphones with different diaphragm tensions and different sensitivities. Using a reference standard and the active coupler, common types of measurement microphones may be calibrated by comparison. The principles are described in 'Infrasound Calibration of Measurement Microphones'. This Appendix describes some details about the applied coupler and measurement system. It also describes calibrations performed on two different Laboratory Standard Microphones, Brüel & Kjaer Type 4160 (IEC 61094–1, LS1) over the frequency range 0.1 to 250 Hz. The method was verified by comparing these results with results obtained by the reciprocity calibration method between 2 and 250 Hz.

Depending on the lowest calibration frequency required, infrasound calibrations generally last for a long time and require couplers with very long time constants of their pressure equalization system. This means that static pressure differences between the ambient and the cavities of the coupler and microphones may become critical and disturb the measurements by displacing the microphone diaphragms, thereby modifying their sensitivities. Such pressure differences may occur especially due to ambient temperature changes or the electrical power supplied to the coupler sound source and microphone preamplifiers. To minimize such effects, the time constant of the coupler venting should be adjusted to match the purpose of the calibration and not be longer than necessary; however, it should not be too short because this would lower the signal and open the coupler for ambient infrasound that, together, may reduce the signal to noise ratio. Frequency responses of the applied coupler are shown in Fig. A1 for different degrees of venting.

Fig. A1. Frequency response of active coupler as a function of venting conditions

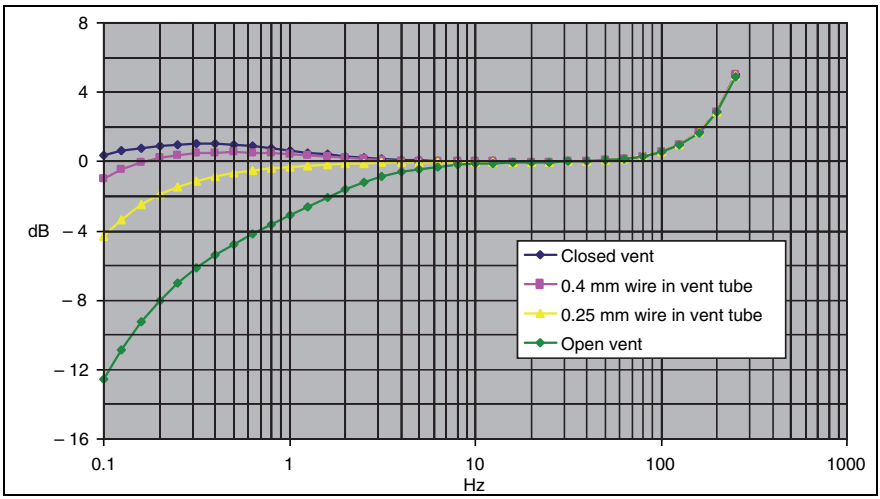

The measurements were performed with a Brüel & Kjaer 2-Channel PULSE Analyzer Type 3560-C. This might work in DC-mode, but it was, in this case, operated in a mode that rolls off by 3 dB at 0.07 Hz. The preamplifiers used, Brüel & Kjaer Type 2673, were modified to have input resistance of 15 GΩ and they were equipped with Adaptors (UC-0211) that contain 100 pF capacitors, which were connected in parallel with the capacitance of the microphones. Together these steps displace the cut-off frequency (i.e., the '–3 dB point') of the measurement channels down to about 0.1 Hz. The gain deviation between the measurement channels was measured by applying the insert voltage facilities of the PULSE analyzer and the preamplifiers and was later equalized, see Fig. A2.

The results of the calibrations performed of the two Laboratory Standard Microphones were compared with results obtained by pressure reciprocity calibrations made in accordance with the principles of the International Standard IEC 61094–2. Even if the present version of this standard is generally considered only to cover frequencies above 20 Hz, some laboratories have, within the last few years, followed its principles and made reciprocity calibrations down to 1 to 2 Hz. So it is for the Danish Primary Laboratory of Acoustics (DFM part) that performed the pressure reciprocity calibrations of the microphones, see Fig. A3A and Fig. A3B. The good agreement between the results supports the methods, which both were applied in a range for which only limited calibration experience is available.

Fig. A2. Schematic for low-frequency measurements of sound and insert voltage gain using two parallel channels of Brüel & Kjaer PULSE Analyzer Type 3560-C

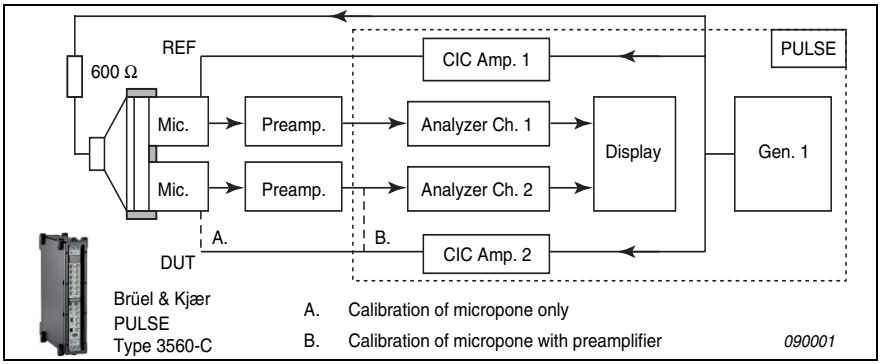

Fig. A3. Comparison of low-frequency calibration results of Type 4160: Serial numbers A) 756412 and B) 1453798

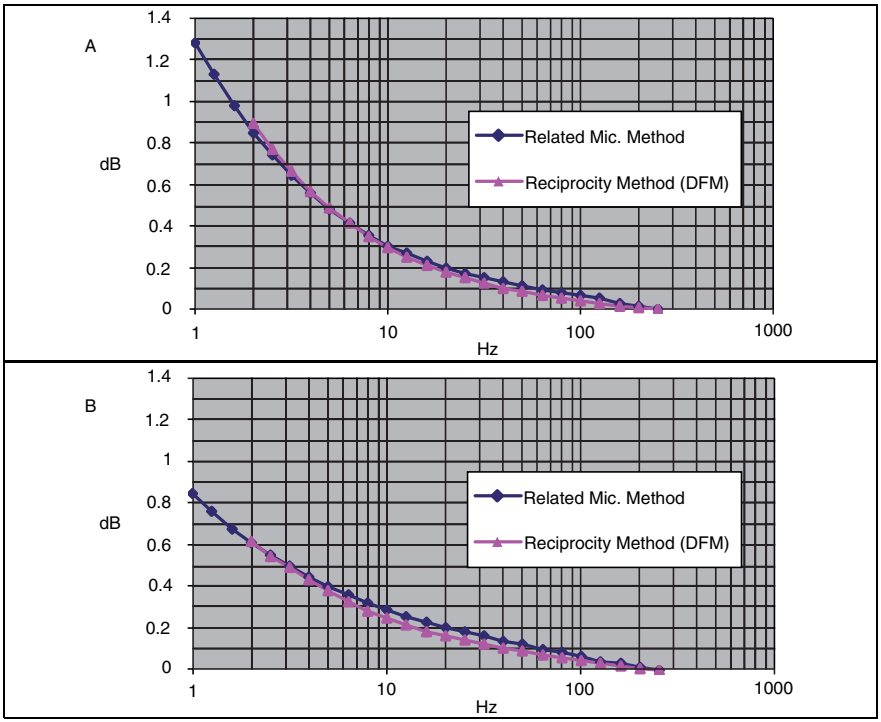

Improved Temperature Specifications for Transducers with Built-in Electronics

Lars Munch Kofoed and Morten Kirkelund[*]

Abstract

In recent years there has been an increasing demand for transducers with built-in electronics that are suitable for temperatures up to 200ºC. Many components are able to operate at higher-than-specified temperatures, but the limitations are often the joining processes, thermal expansion, protection material and electrical specifications. To investigate these processes, several thousand hours of reliability tests have been conducted at temperatures up to 180ºC. The achieved results were very promising and are presented along with new test procedures and limitations.

To predict behaviour at elevated temperatures, analytical models for the critical components have been set up, and based on those models, improvements have been suggested.

Résumé

Les besoins en capteurs avec électronique intégrée pouvant fonctionner à des températures jusqu'à 200ºC augmentent d'année en année. Or, si beaucoup des composants utilisés sont compatibles avec des températures de fonctionnement qui dépassent les spécifications, les limites en la matière sont souvent liées à d'autres raisons : technique de montage, dilatation thermique, matériau de protection et spécifications électriques. Pour étudier tous ces aspects, des milliers d'heures d'essais de fiabilité ont été réalisés à des températures de fonctionnement jusqu'à 180 ºC. Les résultats obtenus, très prometteurs, sont présentés ici conjointement avec les nouvelles procédures d'essai et les nouvelles limites.

* Both authors: Brüel & Kjaer S&V, Naerum, Denmark

Des modèles analytiques ont été élaborés en vue de prévoir le comportement des composants critiques à température élevée. Des améliorations ont été suggérées sur la base d'un examen de ces modèles.

Zusammenfassung

In den letzten Jahren gab es eine steigende Nachfrage nach Sensoren mit integrierter Elektronik, die sich bei Temperaturen bis 200ºC einsetzen lassen. Viele Komponenten können bei höheren Temperaturen arbeiten als in den Spezifikationen angegeben. Die Begrenzungen liegen häufig in Verbindungsprozessen, thermischer Ausdehnung, Schutzmaterial und elektrischen Spezifikationen. Um diese Prozesse zu untersuchen, wurden mehrere tausend Stunden Zuverlässigkeitsprüfungen bei Temperaturen bis 180ºC durchgeführt. Die erhaltenen Ergebnisse waren sehr vielversprechend und werden zusammen mit neuen Testsequenzen und Begrenzungen vorgestellt.

Um das Verhalten bei höheren Temperaturen vorauszusagen, wurden für die kritischen Komponenten analytische Modelle entwickelt und auf der Basis dieser Modelle Verbesserungen vorgeschlagen.

Introduction

For many applications, 120ºC is a sufficient upper tolerance limit, and transducers with built-in electronics and normal components are suitable for the tasks up to that limit. But there is an increasing demand for measurements at temperatures up to 200ºC, and if transducers with built-in electronics are available the same conditioning can be used to make them more flexible.

The purpose of this investigation is to clarify whether it is possible to use amplifiers with standard components for higher temperatures. The investigation includes electronic part rating, joining methods, long-term stability measurement, behaviour modelling at elevated temperatures and proposals for improvements (and testing) to specifications.

The amplifier in this investigation is a standard two wire DeltaTron® amplifier from the Type 4507/08 series.

Components

Capacitors

In a traditional charge amplifier for an accelerometer, the capacitor is a very important component. The feedback capacitor must perform two functions. One is to isolate the high-impedance input from the low-impedance output and the second is to control amplification in the circuit.

Amplification is determined by the capacitance of the capacitor, which needs to be as stable as possible with respect to temperature, as a variation due to temperature will cause a variation in sensitivity of the accelerometer. Hence the formula:

$$V_{\text{out}} = \frac{Q}{C_{\text{feedback}}} \tag{1}$$

where Q is the charge output from the accelerometer and C_{feedback} is the feedback capacitance. This equation shows that the sensitivity changes proportionally with the capacitance of the capacitor.

To make a sufficient isolation between the input and the output, the isolation resistance of the capacitor must be high. A normal accelerometer charge amplifier has an input impedance in the range of a giga-ohm, and an output impedance of just a couple of ohms. A change in isolation resistance will result in a DC drift of the amplifier, which will reduce the dynamic range of the accelerometer and finally drive the accelerometer to overload.

In general, not much can be done with respect to the decrease in insulation resistance. The decrease in resistance tends to follow the Arrhenius equation [1],

$$K = Ae^{\frac{-E_a}{RT}} \tag{2}$$

where:

K is the constant for the process

A is the frequency factor and related to the molecular collision frequency

E_a is the activation energy

T is the temperature in Kelvin

R is the gas constant.

The equation typically indicates doubling of the conductivity per 10ºC. So selecting a capacitor with a high isolation resistance at room temperature is vital. The capacitor's capacitance stability is determined mainly by the type of dielectric constant material used in the capacitor. Materials of the COG type are a major advantage because they have an almost flat temperature coefficient.

Resistors

High-ohmic resistors are used in accelerometer charge amplifiers. Generally, values above several giga-ohms are used to keep the input impedance high. The resistors are part of the lower limiting bandwidth circuit, so the values of the resistors should be kept relatively constant. The lower limiting bandwidth is

$$f_{\text{low}} = \frac{1}{2\pi \cdot C_{\text{feedback}} \cdot R_{\text{bias}} \cdot A_{\text{DC}}} \tag{3}$$

where A_{DC}, is the DC gain.

A thickfilm resistor is a suitable choice. It is not easy to produce these resistors at a stable value, and the typical variation at several giga-ohms is ±40%. However, they tend to be very temperature resistant, due to the fact that they are made of ceramics and glass.

During the design of the high-temperature accelerometer, an experiment was performed to measure the actual variation of the resistance over 200ºC. The variation was found to be less than ±10% with the right resistor.

Component Attachment

A critical issue when producing high-temperature electronics is the attachment of components. It is impossible to use a conventional solder because the melting point is around 175ºC. There are alternative options that can withstand temperatures well above 200ºC, but they cause problems due to the flux that needs to be applied under the soldering process. The flux for high-temperature solders has proven to be very hard to clean after the soldering process. It is absolutely crucial to keep the circuit clean due to the high impedances in the circuit.

Silver epoxy-based adhesives were chosen as the most suitable solution. There are several different types of silver epoxies on the market today that work uninhibited above 200ºC. The adhesive properties of the epoxies are, however, not as good as a solder, but a series of experiments was conducted to identify the best epoxy for the thick film conductive paste.

Semiconductor Components

Many Brüel and Kjær DeltaTron charge amplifiers contain an ASIC. The ASIC is essentially an operational amplifier. This circuit is typically made for operation up to 125ºC, so extensive tests were performed to guarantee operation at 180ºC. Due to the high input impedance, leakage at the input stage is critical. The characteristics of this leakage current are described in the section titled "Leakage Current" on page 38. The leakage current cannot be improved without changing the device – which is not an option.

What can be improved is how the ASIC is mounted and connected to the thick film hybrid. The bonding pads on the ASIC are made of aluminium, and the ASIC is bonded with a gold ball bonding. This generates some issues concerning the intermetallic connections in the circuit.

At temperatures above 125ºC, the formation of $AuAl_2$, begins to pose a problem. This Au-Al phase is popularly called Purple Plague [2]. However, this reaction is also catalyzed by the current running through the bond wire and the chemical composition of the encapsulation covering the ASIC. Nothing was done to avoid the Au-Al connection, but encapsulant type and current passing through the wires were given consideration.

General

A series of amplifiers was made based on the findings of the above considerations. These amplifiers were based on a ceramic thick film with COG capacitors, thick film resistors and Brüel & Kjaer ASICs were mounted using epoxies.

The general strength of the hybrid is very good. The thermal expansion coefficients of the different components and the thick film are very well matched due to the fact that almost all the components are made of different type of ceramics, and the thermal expansion coefficient of the ASIC is close to the thermal expansion coefficient of the ceramics.

Results

After 3000 hours at 180ºC the accelerometers were tested and inspected to determine the general state of the electronics. The two tests were a visual inspection and a shock test. The visual test of the device showed no visual degradation of the amplifiers. The shock test was carried out as 20 shocks of more than 5000 g to ensure that all the components were still attached properly. None of the amplifiers failed at the shock test. There was no test carried out to check for purple plague; this was assumed not to be a problem as none of the bonding failed.

Long-term Stability

In order to measure amplifier stability, as many components as possible should be taken into account. The simplified diagram (see Fig. 1), shows that component change (e.g., value, leakage or voltage offset) will be reflected in bias voltage, V_{out}.

Because the error mechanism's contribution versus temperature differ, a decision was made to perform tests at different temperatures (165, 175 and 180°C) and sensitivities. In order to detect short-term variation in the bias, the logging intervals were set to 1 minute.

It is important to notice that a low bias does not indicate a bad device if the bias is stable; however, it could be outside our specification.

Fig. 1. Simplified two-wire DeltaTron amplifier

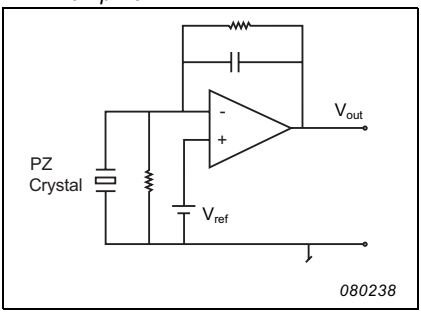

The test was set up as follows:

- Sixty amplifiers mounted in accelerometer housings (without PZ element) in order to take also the mounting into account
- An automatic data logging system was defined to accomodate:
  - Three ovens with fixtures for 20 amplifiers and temperature probes
  - A Voltmeter with 60-channel multiplexer
  - A 60-channel DeltaTron supply
  - A computer with a data logging program.
- All communication between ovens and multiplexer is via RS-232 interface.

The schematic setup is shown in Fig. 2

Fig. 2. Schematic setup

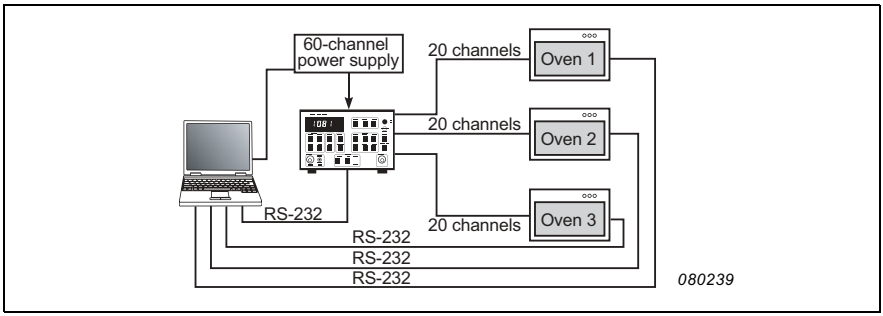

Fig. 3 shows an oven with accelerometers and temperature sensor prepared for test. It was possible to follow the bias over the next 3000 hours.

Fig. 3. Oven with accelerometers (left) and close-up of accelerometers (right)

Results

In order to describe the bias variation versus time, a stability test was carried out. Fig. 4 and Fig. 5 depict accelerometers with different behaviours and a temperature probe placed close to the accelerometers.

Fig. 4. First 60 minutes of testing

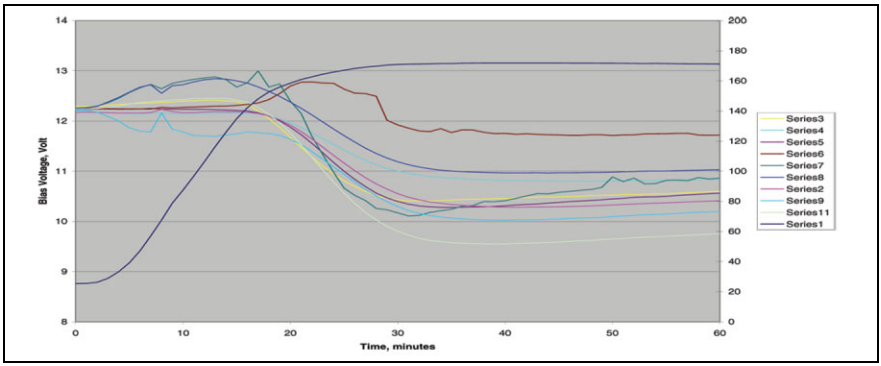

Fig. 4 shows the first 60 minutes after the start of the test. Due to the temperature gradient, varied behaviour is exibited, but after 60 minutes, the values are more stable at a lower bias level. After approximately 24 hours, there is a clearer picture of the stability. Most of the accelerometers have a stable bias at a lower level, but with small changes versus time. A comparison with the temperature probe shows that this has to do with the temperature change in the

Fig. 5. After 24 hours of testing

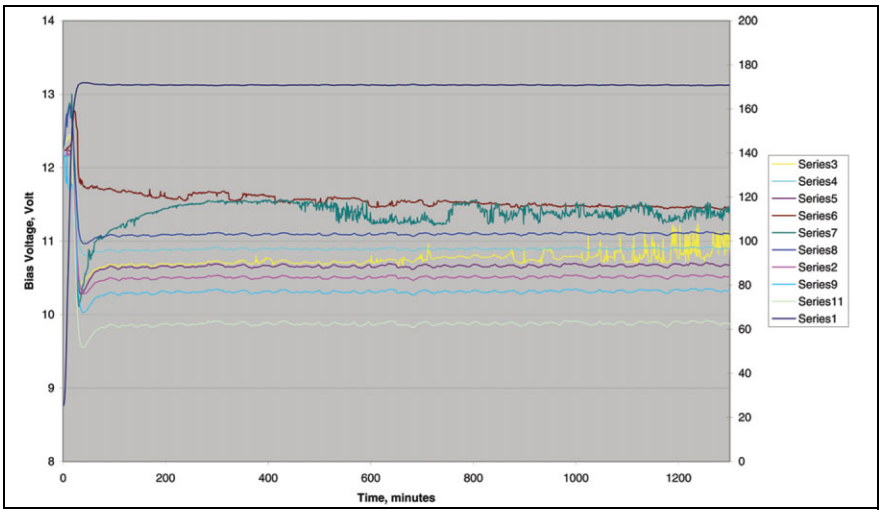

oven. There are also short-term bias steps in the range of a few hundred millivolts or slow variations in the same range. These bias steps do not change the AC amplification, but introduce low-frequency noise, indicating that unstable components might fail and cause a major error. The test was continued for more than 3000 hours, and no further degradation in bias voltage was observed over time. No accelerometers failed after the first 24 hours.

Modelling

Error Contribution to the Bias Voltage Evaluation

The long-term test indicated a clear drop in the bias voltage, and in order to identify the different contributions and come up with proposals for improvements, models were set up for the amplifier behaviour at high temperatures.

The models are based on analytical equations for the critical components and calculations in Mathcad.

A schematic diagram for the two-wire amplifier is shown in Fig. 6

The first step is to calculate the DC output voltage based on the components without the protection diodes and the capacitors (see Eq. 4).

Fig. 6. Schematic of the two-wire DeltaTron amplifier

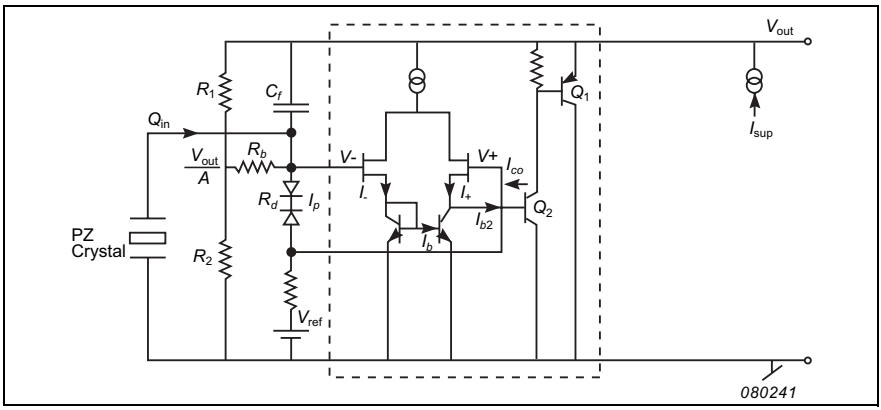

$$V_{\text{out}}(T) = V_{\text{ref}} \cdot \frac{A}{1 + \frac{A}{A_0}} \tag{4}$$

where A_o is open loop gain and A is based on the voltage divider with R1 and R2.

With high open loop gain, A_o= 6000, A= 4.8 and V_{ref} = 2.5 V , V_{out} is 12 V.

The following mechanisms can contribute to bias drop at high temperatures:

- Leakage from the Mosfet input stage
- Leakage in the feed back capacitor
- Offset voltage between the inputs
- Open loop gain
- Variation in the resistance in the protection diodes

If we include the protection diodes as a resistor, $R_d(T)$; an offset voltage, V_{off} ($V_- - V_+$), between the inputs; and a leakage current, $I_g(T)$, at V_- (leakage current at V_+ is not relevant due to the low impedance connection to V_{ref}), we have Equation 5:

$$V_{\text{out}}(T) = \frac{\left[V_{\text{ref}} + V_{\text{off}} \cdot \left(1 + \frac{R_f}{R_d(T)}\right) - I_g(T) \cdot R_f\right] \cdot A}{1 + \frac{A}{A_0} \cdot \left(1 + \frac{R_f}{R_d(T)}\right)} \tag{5}$$

The influence from the added components gives a negligible contribution to the output voltage at room temperature.

The next step is to include temperature behaviour models for the added components.

Leakage Current

The leakage current from the Mosfet depends on the losses in the gate, which in turn depend on the gate area, thickness, dielectric material and voltage across the gate.

The temperature dependency is normally described by Equation 6.

$$I_g(T) = I_{g0} e^{\beta \cdot (T - 273)} \tag{6}$$

where:

$I_{g0} = 10^{-16}$ A ; estimated current at 0ºC

$\beta = 0.07 \text{ deg}^{-1}$

T is the temperature in Kelvin.

A 10ºC temperature increase will change the current by a factor of two. Leakage from the feedback capacitor will follow the same equation.

Protection Diodes

A good approximation to the diode equation is given by Equation 7.

$$I_d(V, T) = I_0 \cdot e^{(-Vg)/V_t} \cdot \left(e^{V/V_t} - 1 \right) \tag{7}$$

$$V_t = \frac{k \cdot T}{q}$$

$q = 1.60 \cdot 10^{-19}$ C

$k = 1.38 \cdot 10^{-23}$ J/K

$V_g = 1.21$ V (energy gap for Silicon)

where:

T is temperature (K)

V is voltage across the diode (V)

I_d is diode current (A)

I_0 is constant for this diode and set to 10^7 A

Two diodes are coupled back to back, and the current, I_p, through the diodes yields:

$$I_p(V,T) = I_s \cdot \left(\frac{1 - e^{V/V_t}}{1 + e^{V/V_t}} \right) \tag{8}$$

$$I_s = I_0 \cdot e^{-V_g/V_t}$$

Fig. 7 shows the protection current of the diode, where V is in millivolts and T is 180ºC.

Based on Equation 8, we are able to calculate the impedance for small signals (Eq. 9) and display the results in Fig. 8.

Fig. 7. Graph of diode protection current

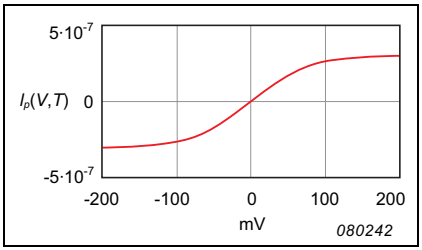

Fig. 8. Small signal impedance

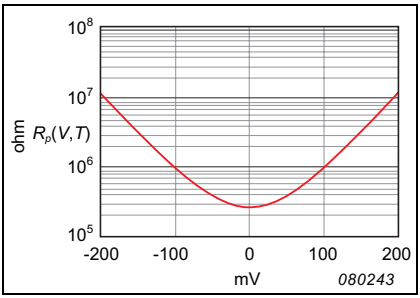

$$R_p(V,T) = \left(1 + e^{V/V_t}\right)^{-2} \cdot e^{V/V_t} \cdot 2 \cdot \frac{I_s}{V_t} \tag{9}$$

where impedance up to $\pm 30\,\text{mV}$ is assumed constant and impedance for $V = 0$ is $R_p(T) = 2 \cdot I_s / V_t$.

Offset Voltage

Due to component processing, there will always be a small random offset voltage, but in this amplifier there was also a few millivolt systematic error.

In order to calculate the offset, the input stage was examined. The current in each arm is:

$$I_{-} = I_e + I_b \tag{10}$$

and

$$I_+ = I_e - I_b + I_{b2} - I_{co} \tag{11}$$

where I_e is the emitter current in the mirror and I_{b2} the current in Q_2

$$I_- - I_+ = 2\,I_b - I_{b2} + I_{co} \tag{12}$$

The difference reflects the imbalance. In this case, the imbalance is positive. The imbalance can be observed at the input as an offset:

$$V_{\text{off}} = V_- - V_+ = -(2\,I_b - I_{b2} + I_{co})/g_m \tag{13}$$

where g_m is the transconductance of the Mosfet. Measurements show offset around – 4 mV.

Open Loop Gain

The open loop gain is approximately 3000 and with the gain A= 4.8, it contributes only with a very small error, but in combination with the other components, we will get a clear contribution.

Calculations

Table 1 gives the error contributions in the amplifier response from the various sources using the expressions given above (Eq. 5).

Table 1. Comparison between simulation and experimental results

Example	Leakage Current	Offset Voltage	Protection Diodes	Open Loop Gain
1	I_g= 0	$V_{\text{off}} = 0$	R_d not included	3000
2	I_g= 0	$V_{\text{off}} = 0$	$R_d = R_d(T)$	3000
3	I_g= 0	$V_{\text{off}} = -4$ mV	$R_d = R_d(T)$	3000
4	$I_g = I_g$T	$V_{\text{off}} = -4$ mV	$R_d = R_d(T)$	3000

Results

The results (see Fig. 9) show clearly that all the errors reduce the output voltage at high temperatures, which would reduce the dynamic range significantly. The question is whether it is possible to improve it.

Fig. 9. Graph of contributions based on Table 1

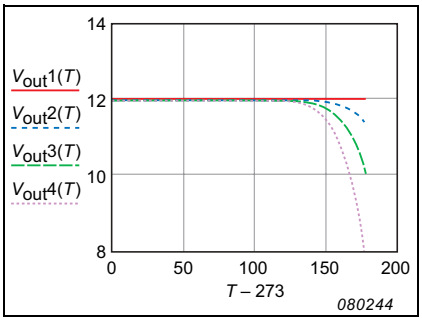

Fig. 10. Version of Fig. 9 substituting +4 mV in place of –4 mV

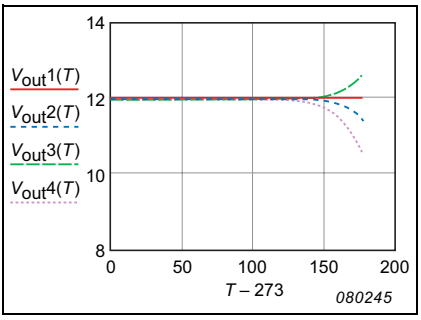

The only parameter that we might be able to change is the offset. If we add a resistor, R between the base of Q_2 and ground (see Fig. 6), we are able to change the balance (see Eq. 14).

$$V_{\text{off}} = -(2\, I_b - I_{b2} + I_{co} - V_{b2}/R)/g_m\,, \tag{14}$$

where g_m is the transconductance of the Mosfet.

If we use +4 mV rather than –4 mV in Equation 5, we achieve the graph shown in Fig. 10.

The result shows clearly that the first two curves are unchanged as expected because V_{off} is not included in the response, while the other two curves show higher output.

The proposed modification is tested with different resistors and shown in Fig. 11. The results show that, with a resistor between 100 and 200 kΩ, it is possible to improve performance.

Conclusions

The conclusions of this study are as follows:

- After thousands of hours of testing at different temperatures, we can conclude that the amplifier components generally have shown very good stability and physical state
- It is not possible to predict high-temperature behaviour at room temperature
- The bias level shift from room temperature to max temperature is explained in the theory and calculations

Fig. 11. Test results after modification

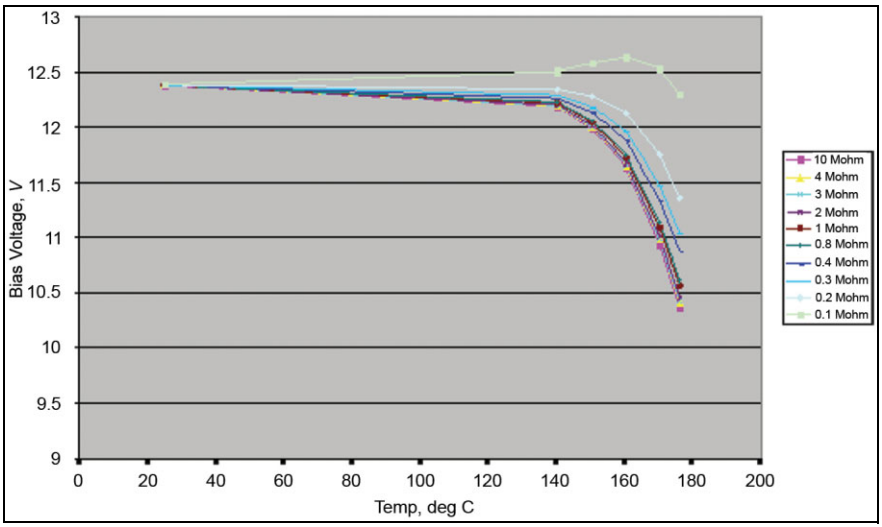

- A low and stable bias is not critical; however, the maximum measuring range will decrease
- Adding an offset voltage to the differential input will reduce the bias drift

Production

In order to avoid unstable accelerometers, a 100% burn-in test at maximum temperature is specified in the production for all accelerometers with traditional built-in electronics and specified for maximum temperatures higher than 160ºC. The test includes checking the bias range and stability.

Reference

[1] S.S. Zumdahl, *Chemical kinetics in chemical principles.* D.C. Heath and Company, Massachusettes – Toronto: 1992.

[2] M. Kirkelund, *Højtemperaturforforstærker til accelerometere*. Brüel and Kjær, Ørsted DTU: 2006.

Previously issued numbers of Brüel & Kjær Technical Review

(Continued from cover page 2)

2 – 1994 The use of Impulse Response Function for Modal Parameter Estimation
Complex Modulus and Damping Measurements using Resonant and Non-resonant Methods (Damping Part II)
1 – 1994 Digital Filter Techniques vs. FFT Techniques for Damping Measurements (Damping Part I)
2 – 1990 Optical Filters and their Use with the Type 1302 & Type 1306 Photoacoustic Gas Monitors
1 – 1990 The Brüel & Kjær Photoacoustic Transducer System and its Physical Properties
2 – 1989 STSF — Practical Instrumentation and Application
Digital Filter Analysis: Real-time and Non Real-time Performance
1 – 1989 STSF — A Unique Technique for Scan Based Near-Field Acoustic Holography Without Restrictions on Coherence
2 – 1988 Quantifying Draught Risk
1 – 1988 Using Experimental Modal Analysis to Simulate Structural Dynamic Modifications
Use of Operational Deflection Shapes for Noise Control of Discrete Tones
4 – 1987 Windows to FFT Analysis (Part II)
Acoustic Calibrator for Intensity Measurement Systems
3 – 1987 Windows to FFT Analysis (Part I)
2 – 1987 Recent Developments in Accelerometer Design
Trends in Accelerometer Calibration
1 – 1987 Vibration Monitoring of Machines

Special technical literature

Brüel & Kjær publishes a variety of technical literature which can be obtained from your local Brüel & Kjær representative.
The following literature is presently available:

- Catalogues (several languages)
- Product Data Sheets (English, German, French,)

Furthermore, back copies of the Technical Review can be supplied as listed above. Older issues may be obtained provided they are still in stock.

HEADQUARTERS: DK-2850 Nærum · Denmark
Telephone: +45 45 80 05 00 · Fax: +45 45 80 14 05
www.bksv.com · info@bksv.com

Brüel & Kjær

BV 0060–11 ISSN 0007–2621